PCCP

Accepted Manuscript

ROYAL SOCIETY OF CHEMISTRY

www.rsc.org/pccp

Functionalized SPIONs: the surfactant nature modulates the self-assembly and cluster formation

Alessandra Luchini,[a,b] Richard K. Heenan,[c] Luigi Paduano[a,b] and Giuseppe Vitiello[b,d,*]

[a] Department of Chemical Sciences, University of Naples "Federico II", Complesso Universitario di Monte S. Angelo, via Cintia 4, 80126 Naples, Italy.

[b] CSGI, Consorzio Interuniversitario per lo Sviluppo dei Sistemi a Grande Interfase, Via della Lastruccia 3, 50019 Sesto Fiorentino (Florence), Italy.

[c] ISIS-STFC, Rutherford Appleton Laboratory, Chilton, Oxon OX11 0QX, United Kingdom.

[d] Department of Chemical, Materials and Production Engineering, University of Naples "Federico II", Piazzale Tecchio 80, 80125 Naples, Italy.

**corresponding author*
e-mail: giuseppe.vitiello@unina.it; Tel: +39 081 76 85 975 – Fax: +39 081 76 82 595

Abstract

SuperParamagnetic Iron Oxide Nanoparticles (SPIONs) represent a suitablesystem for several applications especially in nanomedicine. Great efforts have been devoted to the design of stable and biocompatible functionalized SPIONs suitable for diagnostics and drug delivery. Particularly, zwitterionic-surfactant functionalized SPIONs, obtained through a coating strategy based on hydrophobic interaction, are promising systems for biomedical applications. The size of functionalized SPIONs has emerged as a crucial parameter determining their fate in living organisms. However, not all the proposed functionalization strategies lead to monodispersed systems and SPIONs clustering often occurs. In this study, we report a systematic investigation on different surfactant-functionalized SPIONs in order to explore the possibility of tuning the particle size by choosing an appropriate amphiphilic molecule. By combining Small-Angle Neutron Scattering (SANS) and Dynamic Light Scattering (DLS) analysis, we have provided a detailed description of the functionalized SPION structure. Furthermore, we have also related the surfactant aggregation properties, i.e. the Critical Micelle Concentration (CMC), with its efficiency in coating SPION surface, which eventually causes cluster formation. On this basis, the present study contribute to furnish decisive information to define synthetic strategies able to tune functionalized-SPIONs design.

Keywords: SPIONs, surfactant, clusters, hydrophobic interaction, nanomedicine.

1. Introduction

SuperParamagnetic Iron Oxide Nanoparticles (SPIONs), thanks to their super-paramagnetic properties, are perfect candidates for different technological applications[1-3]. SPIONs can be used as extractants for the removal of target molecules from aqueous media by exploiting magnetic precipitation techniques [4]. Nanomagnetic systems[5], such as in high density magnetic tape recording[6] were also produced using SPIONs. In addition, SPIONs are extensively utilized as catalysts owing to their high specific surface and accessibility.[7] As an example, SPIONs resulted to be more effective than conventional large-size iron oxide particles for the oxidation of CO and the oxidative pyrolysis of biomass.[8] However, the most popular SPIONs application is in nanomedicine, as Magnetic Resonance Imaging (MRI) contrast agents [9, 10], but also as multifunctionalizable nanoplatforms for multimodal imaging[11, 12], and drug carriers [9, 13, 14]. Recently different synthetic protocols were proposed for the preparation of SPIONs [15, 16], among which the thermal-decomposition method represents a robust route to obtain nanoparticles with a narrow size distribution.[17]

In order to suitably use SPIONs for most of the listed applications it is mandatory to obtain them as a stable aqueous suspension. Thus, since the thermal decomposition method leads to SPIONs coated with a hydrophobic organic layer, needed to control SPION growth, a further functionalization step is required to stabilize them in water media. Two different functionalization approaches are commonly reported in the literature, which are based on the ligand exchange or the hydrophobic interaction[14, 18, 19]. The ligand-exchange approach requires the selection of an appropriate functionalizing molecule. This molecule must have high affinity for the iron oxide surface, and must be able to substitute the preexisting coating. Thus, hydrophobic SPIONs can be converted to water-soluble functionalized SPIONs by choosing a hydrophilic molecule. Examples are hydrophilic ligands with anchoring groups such as dopamine, carboxylic acids, phosphines and amines, all of which have good affinity for iron oxide surfaces.[20] This approach can produce a stable organic layer, strongly bound to the nanoparticle surface. In general, the ligand-exchange approach needs a purification step to remove the organic molecules originally binding the SPION surface from the suspension.

On the other hand, in the functionalization through hydrophobic interaction, the organic shell is kept and exploited to introduce on the SPION surface a second layer composed by amphiphilic molecules. This second amphiphilic layer is bound to the organic shell initially present on the SPION surface by means of the hydrophobic interaction. Hence, the amphiphilic coating can be achieved through redispersion of the precipitated hydrophobic SPIONs with an aqueous solution

containing the functionalizing agents. As an alternative, the same functionalization strategy can be enacted at the interface between water and an organic solvent.[20]

The interesting advantage of SPION functionalization through hydrophobic interaction is that different molecules can be easily and concurrently introduced on the SPION surface [21]. Thus, it is a suitable approach to obtain functionalized SPIONs able to combine different functionalities, such as contrast agents for imaging techniques or drug carriers without any substantial molecular modifications or variations in the functionalization protocol.

SPION functionalization is not simply required to produce stability in aqueous media, but it is fundamental to improve the biocompatibility of the nanoparticles. At this purpose, both the discussed functionalization strategies have been successfully adopted to introduce on the SPION surface a large variety of biocompatible molecules, such as proteins[22], nucleic acids[23], polymers[24, 25] or surfactants[26, 27]. Among them, it is worth to cite the case of PolyEthyleneGlycol (PEG) molecules modified with phospholipids, which can be introduced on the SPION surface leading to good performances as MRI contrast agents[28]. PEG-functionalized SPIONs have been approved by the United States Food and Drug Administration (FDA) for the diagnostic application[28]. However, recently SPIONs functionalized with zwitterionic surfactants, exhibiting both a positively and negatively charged group in their polar head, were obtained both *via* ligand exchange or hydrophobic interaction. This kind of functionalized SPIONs have been proposed as a valuable alternative to PEG-functionalized SPIONs[18, 29-32]. Indeed, as reported by Groult *et al.*, zwitterionic-surfactant functionalized SPIONs were obtained by decorating the SPIONs surface through hydrophobic interaction with phosphatidylcholine, a bi-tailed surfactant. These functionalized SPIONs are characterized by a longer circulation time and larger stability in a wide pH-*range*[18]. Muro *et al*. and Estephan *et al.* have also reported great advantages of zwitterionic-surfactant functionalized SPIONs with respect to PEG-functionalized SPIONs, being more stable at high salt concentration and less prone to adsorb proteins[30, 32]. Nevertheless, depending on the zwitterionic-surfactant used for SPIONs the functionalization, of the SPION clustering might occur.

Here, we report the systematic characterization by means of Small Angle Neutron Scattering (SANS) and Dynamic Light Scattering (DLS) of three different surfactant-functionalized SPIONs~~,~~. The aim of the performed characterization was to provide a deep insight into the structure of the organic coating of the functionalized SPIONs as well as the relation between the surfactant aggregation properties and the cluster formation. SPIONs with 6 nm radius and narrow size distribution were synthesized through the thermal decomposition method and decorated with the two zwitterionic phopshocholines, 1-palmitoyl-2-hydroxy-*sn*-glycero-3-phosphocholine (16LPC) and 1-stearoyl-2-hydroxy-*sn*-glycero-3-phosphocholine (18LPC), as well as the cationic surfactant

cetyltrimethylammonium bromide (CTAB). The two zwitterionic phosphocholines belong to the class of lysophospholipids, which are amphiphilic single-chain molecules included into cells membranes.[33] Specifically, 16LPC and 18LPC share the same hydrophilic head but differ for the hydrophobic tails. On the other hand, CTAB and 16LPC share the same hydrophobic region but differs for the polar head. Hence, by comparing the structural characterization performed on the SPIONs functionalized with three different surfactants, the clustering tendency was systematically studied. In particular, it resulted to be a function of the hydrophobic and hydrophilic structure of the surfactant. Thus the surfactant efficiency in coating the SPIONs was related to its aggregation properties.

The fate of nanoparticles in a living organism is determined by their coating but also by their size.[28] Thus, considering to the great potentiality of zwitterionic-functionalized SPIONs, we believe that the present work contributes to establish a rational design of functionalized SPIONs, according to the aggregation properties of the used surfactants.

2. Experimental section

2.1 Materials

Iron (III) acetylacetonate ($Fe(acac)_3$, 99%), 1,2-hexadecanediol ($C_{14}H_{29}CH(OH)CH_2(OH)$, 90%), oleylamine (OAM, $C_9H_{18}=C_9H_{17}NH_2$, 70%), oleic acid (OA, $C_9H_{18}=C_8H_{15}$-COOH, 99%), diphenyl ether ($C_{12}H_{10}O$, 99%), ethanol (≥98%), cetyltrimethyl ammonium bromide (CTAB $CH_3(CH_2)_{15}N(Br)(CH_3)_3 \geq 99\%$) and deuterated water ($D_2O$ 99.9%D) were purchased from Sigma Aldrich. 1-stearoyl-2-hydroxy-3glicero-sn-phosphocholine (18LPC $C_{26}H_{54}NO_7P$, >99%) and 1-palmitoyl-2-hydroxy-*sn*-glycero-3-phosphocholine (16LPC,$C_{24}H_{50}NO_7P$,>99%) were purchased from AvantiPolar Lipids Inc.

2.2 Preparation of functionalized SPION suspensions

SPIONs were synthesized with a first coating layer composed by oleic acid and oleylamine, according to the thermal decomposition method proposed by Sun et al.[17]. According to this protocol, 0.355 g of $Fe(acac)_3$, 1.29 g of 1,2-hexadecanediol, 1.0 mL of oleylamine, 1.0 mL of oleic acid and 10 mL of diphenyl ether, were mixed together in a three-neck flask. The solution was heated at 200 °C under argon atmosphere and vigorous stirring. After 2 h at reflux, the flask was removed from the heater and cooled to room temperature. In order to remove the undesired components, the suspension was treated with ~ 10 mL of ethanol and centrifuged at 7000 rpm for 20 min. SPIONs coated with oleic acid and oleylamine, obtained as a solid precipitate, have been then re-dispersed in cyclohexane. The iron concentration in the obtained nanoparticles was

evaluated by means of Inductively Coupled Plasma Mass Spectroscopy (ICP-MS) as corresponding to 2 mg/mL.

Stable aqueous suspensions of SPIONs were obtained by functionalizing them through hydrophobic interaction with the three different surfactants: 18LPC, 16LPC and CTAB. According to our recently proposed protocol[34], 18LPC, 16LPC and CTAB were dissolved in D_2O in order to obtain three independent surfactant solutions with a concentration of $4 \cdot 10^{-3}$ m. 1 mL of SPION cyclohexane suspension was stratified over 1 mL of each of the surfactant solutions. The resulting biphasic systems were sonicated at 50 °C for about 2h in order to promote cyclohexane evaporation and the transfer of the SPIONs in the aqueous phase, where they are stabilized by the surfactant coating. Indeed, due to the hydrophobic interaction the surfactant molecules orient themselves with the hydrophobic tail in the direction of the oleic acid and oleylamine layer, while the hydrophilic head is exposed toward the solvent. The adopted functionalization strategy does not require any purification step leading directly to the obtainment of the functionalized SPIONs. The zwitterionic-surfactant functionalized SPIONs (z-potential -2.2 ± 0.8 mV) were prepared with 18LPC or 16LPC molecules named hereafter respectively as 18LPC/SPIONs and 16LPC/SPIONs. On the other hand, cationic-surfactant functionalized SPIONs (z-potential +50 ± 1 mV) were prepared with CTAB molecules and are named hereafter as CTAB/SPIONs. Samples were prepared in D_2O for the SANS experiments and the same samples were also analyzed at DLS. In this latter case, the diffusion coefficients were corrected for the isotopic effect.

2.3 Dynamic Light Scattering (DLS)

DLS measurements were performed with a home-made instrument composed by a Photocor compact goniometer, a SMD 6000 Laser Quantum 50 mW light source operating at 5325 Å, a photomultiplier (PMT-120-OP/B) and a correlator (Flex02-01D) from *Correlator.com*. All measurements were performed at (25.00 ± 0.05) °C with temperature controlled through the use of a thermostat bath. In DLS, the intensity autocorrelation function, $g^{(2)}(t)$, is measured for the instrument configuration corresponding to the scattering angle of 90°. The intensity autocorrelation function is related to the electric field autocorrelation function, $g^{(1)}(t)$, indicated in equation 1 as the inverse Laplace transform of the distribution of the relaxation rate Γ, $A(\Gamma)$, used to calculate the translational diffusion coefficient $D = \Gamma / q^2$:[35]

$$g^{(1)}(t) = \int_0^\infty A(\Gamma)\, \mathrm{e}^{-\Gamma \tau}\, \mathrm{d}\Gamma \qquad (1)$$

where q is the modulus of the scattering vector $q = 4\pi n_0 / \lambda \sin(\theta/2)$, $n_0 = 1.33$ is the refractive index of the solution, λ is the incident wavelength and θ represents the scattering angle. Inverse Laplace transforms were performed using a variation of CONTIN algorithm incorporated in Precision Deconvolve software[36].

For spheres diffusing in a continuum medium at infinite dilution, in the approximation of spherical objects, the diffusion coefficient is related to the hydrodynamic radius R_h, through the Stokes–Einstein equation:

$$R_h = \frac{kT}{6\pi\eta_0 D} \tag{2}$$

where k is the Boltzmann constant, T is the absolute temperature and $\eta_0 = 0.89cP$ is the solvent viscosity. For non-spherical particles, R_h represents the radius of a spherical aggregate with the same diffusion coefficient measured. In the present system due to the high dilution it is possible to make the approximation that $\eta \cong \eta_0$, where η represents the solution viscosity. In this hypothesis, equation (2) can be reasonably used to estimate the averaged hydrodynamic radius of the particles.[37-39]

2.4 Small Angle Neutron Scattering (SANS)

SANS measurements were performed at 25°C with the Loq instrument located at ISIS Science and Technology Facilities Council, in Chilton (UK). The instrument is characterized by a fixed two-dimensional detector positioned at 4 metres from the sample, which can detect the positions and times of arrival of the scattered neutrons. This configuration allowed collecting data in a range of the scattering vector modulus q (defined as for DLS above) between 0.008 $Å^{-1}$ and 0.221 $Å^{-1}$ using neutrons of wavelengths 2.2 to 10 Å simultaneously by time of flight. The investigated systems were containedin a closed quartz cell, in order to prevent the solvent evaporation. The raw data were then corrected for background and empty cell scattering.

The obtained absolute scattering cross sections $d\Sigma/d\Omega$ data were plotted as function of q. Generally, the dependence of $d\Sigma/d\Omega$ from the scattering vector can be summarized as in equation 3.

$$\frac{d\Sigma}{d\Omega} = \phi_p V_p P(q) S(q) + bkg \tag{3}$$

where ϕ_p, V_p, $P(q)$, $S(q)$ represent the volume fraction of the particles, the particle volume, the form and the structure factor of the scattering particles respectively, while bkg is the incoherent and

inelastic part of the scattered cross section, largely dependent on any hydrogen present. The form factor is responsible for the shape, the size, the size distribution of the scattering particles, while a contribution of the structure factor can be considered when an inter-particle correlation exists. The structural information contained in both the form and the structure factor can be extracted by choosing an appropriate model to fit the experimental data[38].

3. Results

3.1 SPIONs functionalized with zwitterionic surfactants.

Functionalized SPIONs are composed by an inorganic inner core and an organic outer shell. Thus, in order to characterize their structure, it is crucial to choose a technique sensitive with respect to the different components. For this purpose, neutrons represent the perfect probe, since both the iron oxide core and the organic shell can be detected, and in particular the organic molecules in the SPION coating present a good contrast with respect to the solvent. Thus, the potential effect of the surfactant structure on the packing of the amphiphilic molecules in the outer organic shell can be evaluated.

SANS measurements were performed on SPIONs functionalized with the two zwitterionic surfactants, 18LPC and 16LPC. SANS data analysis was supported and complemented by means of DLS characterization underlining the eventual presence of large aggregates. In Figure 1a, SANS experimental data collected for the 18LPC/SPION suspension are reported together with the fitting curve. The suspension was considered as composed by a single distribution of polydispersed spherical particles with core-shell structure, according to equation 3 and the form factor reported in equation 4.

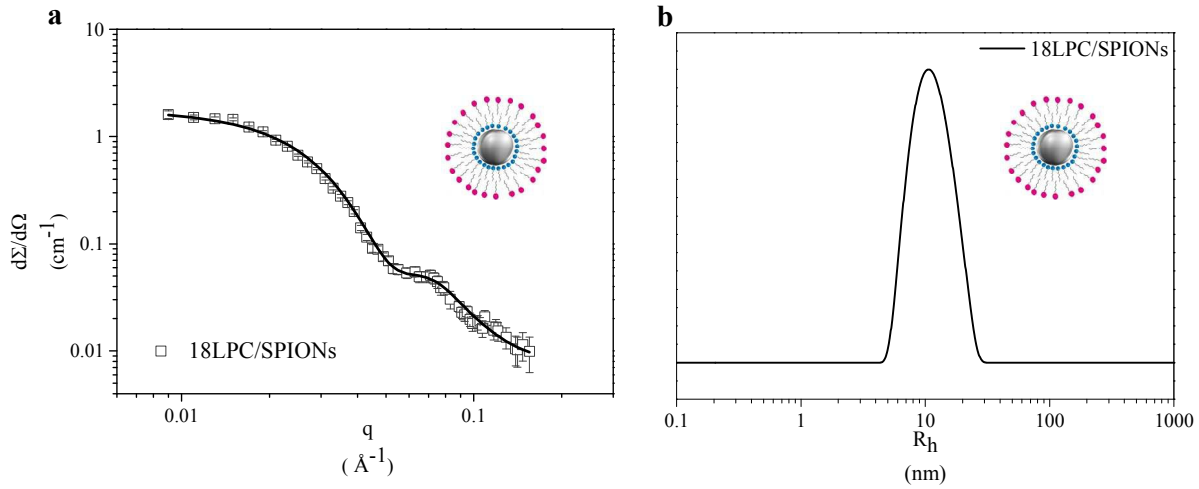

Figure 1: SANS experimental data together with the fitting curve suspension (panel **a**) and hydrodynamic radius distribution obtained from DLS measurements (panel **b**) for 18LPC/SPION suspension.

$$P_{core\text{-}shell}(q) = \frac{1}{V_p^{\,2}}\left[3V_{core}(\rho_{core}-\rho_{shell})\frac{\left[sin(qr_{core})-qr_{core}cos(qr_{core})\right]}{(qr_{core})^3} + 3V_{shell}(\rho_{shell}-\rho_{D_2O})\frac{\left[sin(qr_{shell})-qr_{shell}cos(qr_{shell})\right]}{(qr_{shell})^3}\right]^2 \quad (4)$$

The scattering length densities of the inorganic core and external shell were calculated according to their composition and molecular volume as: $\rho^{neutron}_{Fe_3O_4} = 6.9\times10^{-6}\,\text{Å}^{-2}$ (core), $\rho^{neutron}_{oleicacid} = 7.8\times10^{-8}\,\text{Å}^{-2}$ (inner layer), $\rho^{neutron}_{oleylamine} = -1.7\times10^{-7}\,\text{Å}^{-2}$ (inner layer), $\rho^{neutron}_{18LPC} = 2.9\times10^{-7}\,\text{Å}^{-2}$ (outer layer) and $\rho^{neutron}_{D_2O} = 6.3\times10^{-6}\,\text{Å}^{-2}$. The optimized parameters obtained from the analysis of the collected SANS data are summarized in Table 1.

The good match between the experimental data and the fitting curve confirmed that the 18LPC/SPIONs are indeed characterized by a core-shell structure. In particular, the inorganic-core radius (r_{core}) resulted to be ~3 nm, while the organic shell, composed by two amphiphilic layers, the inner one of oleic acid and oleylamine and the outer one of 18LPC, exhibited ~4 nm thickness (d_{shell}), in perfect agreement with our previous results[21]. The polydispersity on both the inorganic-core radius and organic-shell thickness was calculated considering a Schulz distribution for both parameters. Generally, the polydispersity index associated to a Schulz distribution is defined as the ration between the root mean square deviation of the distribution and its mean value, as reported elsewhere.[40] Thus, together with the r_{core} and d_{shell}, also the polydispersity indices p_{core} and p_{shell} were optimized.

We also estimated the volume fraction of the solvent in the outer organic shell as corresponding to 0.10. The solvent volume fraction was calculated by considering the fitted $\rho_{organic\text{-}shell}$ value as due to the sum of the scattering length density of the pure organic shell plus the D_2O scattering length density weighted by their respective volume fractions.

The 18LPC/SPION suspension was also characterized by means of DLS measurement to investigate the SPION aggregation state. As reported in Figure 1, the 18LPC/SPION suspension is indeed composed by a single population of particles with a mean hydrodynamic radius of about 10 nm. The hydrodynamic radius is calculated by applying Stokes-Einstein relation (equation 2) to the particle mean diffusion coefficient. Thus, by considering the solvation shells that are diffusing with the particle, it is possible to conclude that the estimated hydrodynamic radius of 18LPC/SPIONs (10 nm) is in agreement with the total radius (~6 nm), core radius (2.7 nm) plus shell thickness (3.6 nm), obtained from SANS data analysis.

SANS experiment was performed also on the 16LPC/SPION suspension, as shown in Figure 2a. The collected scattering profile resembled the one observed for the18LPC/SPION suspension. Indeed, the spherical core-shell model, with the polydispersity on both the inorganic radius and the organic shell, showed also for 16LPC/SPIONs a good agreement with the experimental data. Thus, the parameters reported in Table 1 were optimized by applying equation 4, considering the same scattering length density values used for 18LPC/SPION data analysis, but with the scattering length density of the outer shell $\rho_{16LPC}^{neutron} = 2.5\times10^{-7}\,\text{Å}^{-2}$.

16LPC/SPIONs and 18LPC/SPIONs were prepared from the same SPION cyclohexane suspension, and thus, as expected, the inorganic core radius together with the corresponding polydispersity index estimated from the SANS data analysis was the same within the reported errors. The organic shell thickness resulted also to be, within the error, the same as for 18LPC/SPIONs. This result is reasonable since 16LPC molecule differs from 18LPC one only for $2CH_2$ groups in the acyl chain, which means a few Å in terms of the hydrophobic tail length. Interestingly, the solvent volume fraction in the organic shell resulted to be about 0.35, larger than the water amount resulted to be present in the case of 18LPC/SPION. The high solvent content in the outer shell suggests that the 16LPC molecules are not closely packed in the functionalized SPIONs organic shell.

The results obtained from SANS data analysis were compared with the DLS measurements. In Figure 2b, the intensity distribution of the scattering particle hydrodynamic radius is reported. 16LPC/SPIONs suspension was not simply composed by the single functionalized nanoparticles, but also a larger population was detected showing a mean hydrodynamic radius of about 50 nm. According to our previous results on functionalized SPIONs[34], this population was interpreted as SPION clusters. Owing to their large size and small concentration with respect to the single functionalized SPIONs, SPION clusters were not detected in the *q*-range explored during the SANS experiment, even if the increasing slope of the curve at small *q* values might suggest their presence.

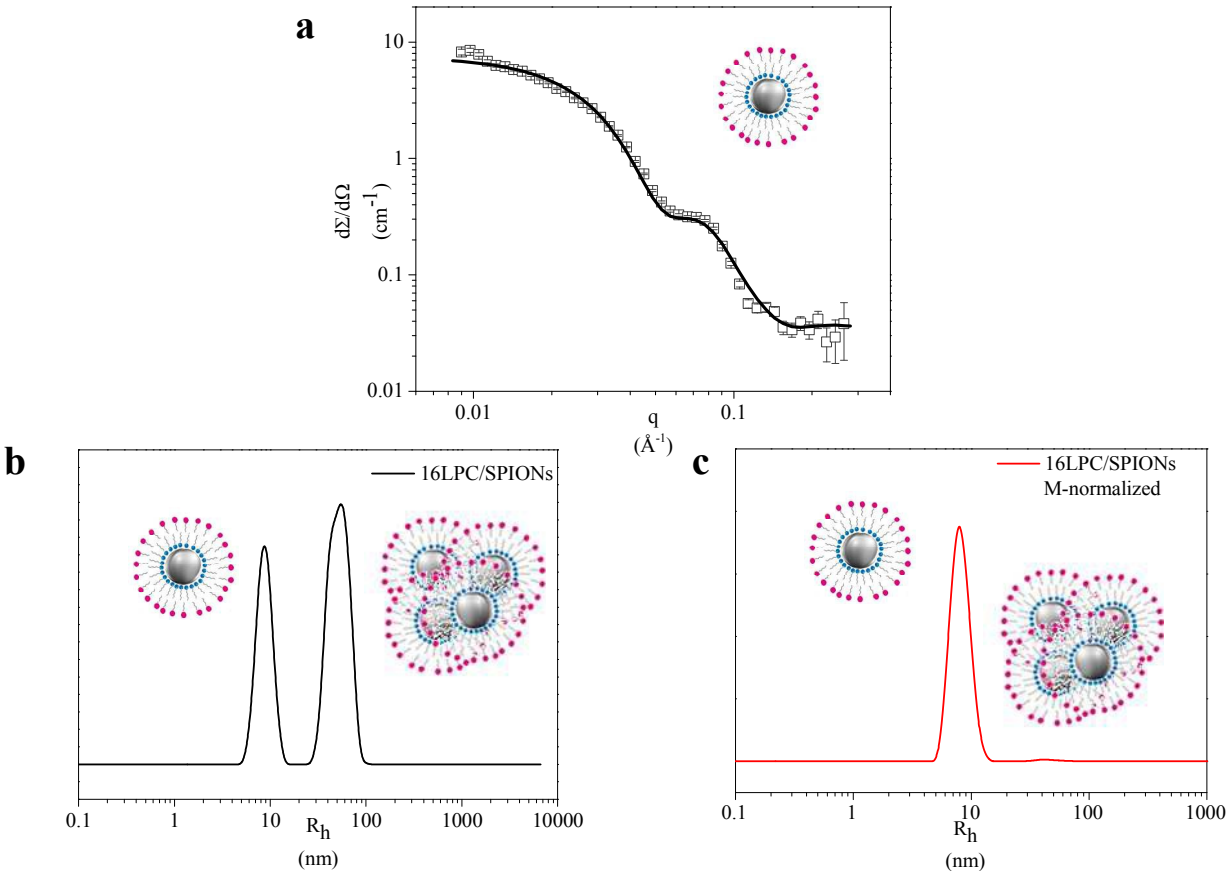

Figure 2: SANS experimental data together with the fitting curve suspension (panel **a**) and hydrodynamic radius distribution obtained from DLS measurements (panel **b**) for 16LPC/SPION suspension. In panel**c** the hydrodynamic radius distribution was normalized for the particle mass.

The scattered intensity measured in the DLS experiment depends on both the mass squared and the concentration of the scattering objects. However, the distribution reported in Figure 2b, can be converted in a concentration distribution by normalizing the scattering intensity for the mass (M) squared of the scattering particle.[36] In the present case, we are dealing with spherical objects[34] so that $M \approx kR_h^3$ where k is a constant. The normalized intensity distribution of the hydrodynamic radius is reported in Figure 2c, showing that the actual contribution of the clusters is very low. This corresponds to about 1% of the total number of scattering particles.

	18LPC/SPIONs	16LPC/SPIONs
r_{core} (nm)	2.7 ± 0.2	2.5 ± 0.3
p_{core}	0.27 ± 0.02	0.29 ± 0.03
d_{shell} (nm)	3.6 ± 0.1	3.7 ± 0.2
p_{shell}	0.19 ± 0.01	0.20 ± 0.01
% solvent	10 ± 1	35 ± 3
D (cm^2s^{-1}) × 10^7	2.34 ± 0.08	2.76 ± 0.14
R_h(nm)	10 ± 1	9 ± 1
$D_{cluster}$ (cm^2s^{-1}) × 10^7	---	0.482 ± 0.55
$R_{h,cluster}$ (nm)	---	51 ± 6

Table 1: Measured and optimized parameters from SANS and DLS measurements for 18LPC/SPION and 16LPC/SPION suspensions.

3.2 SPIONs functionalized with cationic surfactant.

Combined SANS and DLS characterization was performed also for SPIONs functionalized with the cationic surfactant CTAB. In Figure 3a, SANS experimental data are reported together with the corresponding fitting curve. The scattering length density of CTAB was calculated as $\rho_{CTAB}^{neutron} = -1.58 \times 10^{-7}\,\text{Å}^{-2}$. The SANS data pattern in the low-q region was significantly different from the ones collected for 18LPC/SPIONs and 16LPC/SPIONs. The difference was interpreted as produced by the presence of large SPION clusters, whose Guinier region, sensitive to the particle size, was not detectable in the explored q-range. According to this interpretation, the model used to fit the experimental data, was composed by the sum of two different form factors, accounting for the scattered intensity raised from the single functionalized SPIONs and the SPION clusters.

$$I(q) = \varphi_{core-shell} V_{sphere} P_{core-shell} + F(q) + bkg \quad (5)$$

where $P_{core\text{-}shell}$ is defined by equation 4 and $F(q)$ is defined as following:

$$F(q) = A|q|^{-m} \quad (6)$$

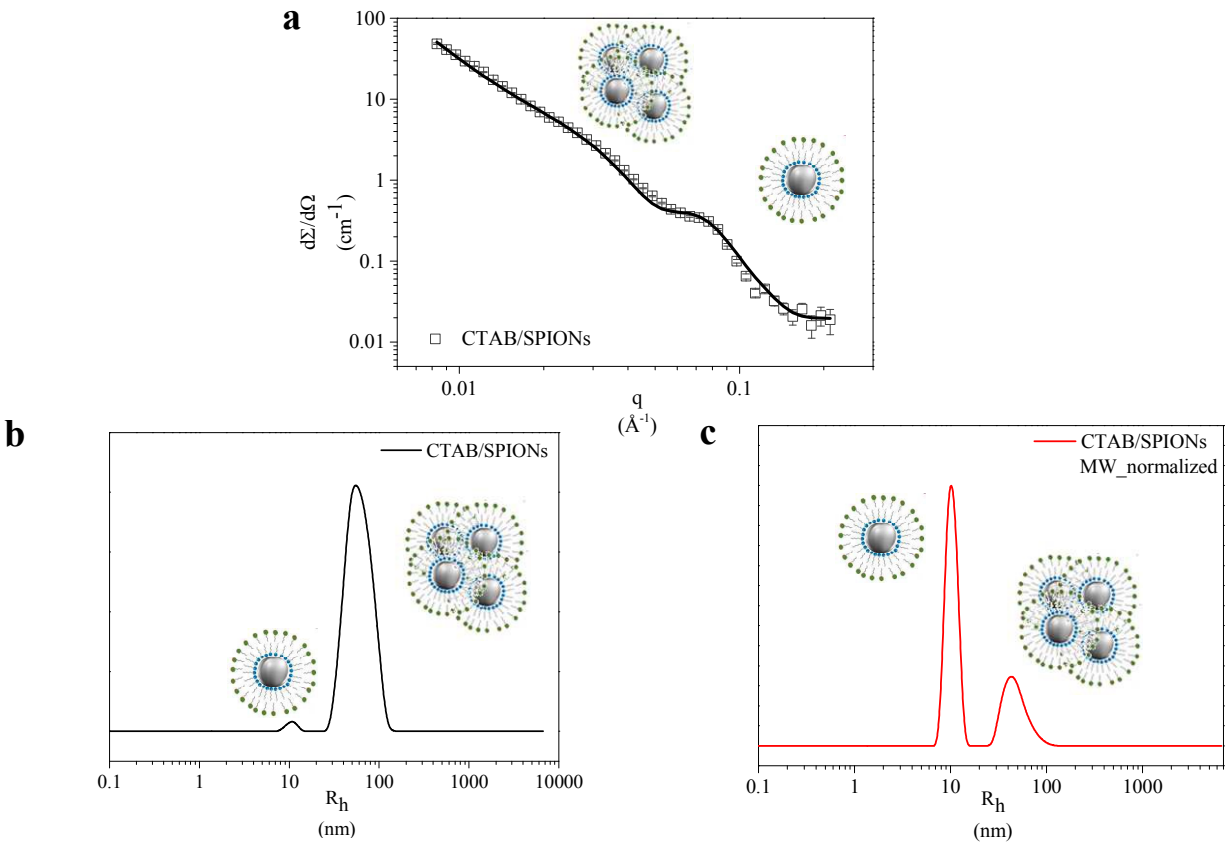

Figure 3: SANS experimental data together with the fitting curve suspension (panel **a**) and hydrodynamic radius distribution obtained from DLS measurements (panel **b**) for CTAB/SPION suspension. In panel **c** the hydrodynamic radius distribution was normalized for the particle mass.

For the single CTAB/SPIONs, the core-shell structure form factor with polydispersity on both the inorganic core and the organic shell, represents the best interpretation of the functionalized SPION structure, as in the case of 16LPC/SPIONs and 18LPC/SPIONs. Indeed, by comparing the parameters reported in Table 1, it is possible to conclude that, even if the structural parameters of the single functionalized SPIONs are not sensibly affected by the surfactant, the solvent volume fraction in the outer shell was found furtherly increased in the case of CTAB. This evidence is in agreement with the higher solvation of CTAB molecules, but also suggests that the surfactant molecules are probably less closely packed with respect to 18LPC. Both these effects can be ascribable to the positive charge exhibited by the CTAB polar head, and to the electrostatic repulsion occurring between these positive headgroups which does not favour the formation of a more compact layer.

CTAB/SPIONs				
r_{core} (nm)	p_{core}	d_{shell} (nm)	p_{shell}	% solvent
2.4 ± 0.3	0.29 ± 0.04	3.9 ± 0.4	0.22 ± 0.02	55± 2

D (cm^2s^{-1}) $\times 10^7$	R_h (nm)	$D_{cluster}$ (cm^2s^{-1}) $\times 10^7$	$R_{h,cluster}$ (nm)
2.15 ± 0.41	11 ± 2	0.43 ± 0.08	51 ± 1

Table 2: Measured and optimized parameters from SANS and DLS measurements.

On the other hand, the cluster contribution to the scattered intensity was accounted by introducing a power law form factor (equation 7). Thus, the optimized value of the exponent *m* corresponding to about 3 was obtained for the increment of the scattered intensity at low *q*. The significant contribution of the cluster to the scattered intensity in the SANS measurement, suggests that a larger amount of clusters is present within the suspension with respect to 16LPC/SPIONs. In principle, since CTAB/SPIONs are charged nanoparticles, electrostatic interactions among the SPIONs should be taken into account in the interpretation of the experimental data. However, since diluted suspensions of functionalized SPIONs were characterized by both SANS and DLS, it is reasonable to consider that the interparticle interactions do not strongly affect the collected data.

DLS experiments were performed to characterize the cluster size in terms of their hydrodynamic radius. We note that in principle the hydrodynamic radius of the CTAB/SPIONs should be evaluated from the diffusion coefficients of the pure nanoparticle, i.e. eliminating the effect of counter-ion on the experimental diffusion coefficients. However such effect is more effective as the concentration of the charge aggregates is quite large, as well discussed in literature.[41-43]

As showed in Figure 3c, the two populations composing the CTAB/SPION suspension present very similar hydrodynamic radius values with respect to the 16LPC/SPION suspension. However, cluster contribution to the scattered intensity is definitely higher about 30% (scattering particle number density).

Discussion

The structure of SPIONs functionalized with different amphiphilic molecules was characterized with a particular focus on both the inorganic and organic components, with the aim of evaluating the clustering tendency of the functionalized SPIONs. SANS data were initially collected to achieve a detailed description of the structure of the single functionalized SPIONs. Both the inorganic-core radius and the organic-shell thickness were evaluated and subsequently compared for all the investigated functionalized SPIONs. We have observed that the structure of the single

functionalized SPIONs was not globally affected by the surfactant used during their functionalization. Indeed, the size of the organic shell was roughly the same. However, a considerably different solvent fraction in the organic shell was calculated. We postulate that this result is produced by 16LPC and CTAB molecules forming a less compact organic shell on the SPION surface with respect to 18LPC. Parallel to this indication, our experimental results have also demonstrated that 18LPC/SPIONs were obtained as a monodispersed aqueous suspension while, in the case of both 16LPC and CTAB/SPIONs, cluster formation was observed with a larger amount of clusters being present in the CTAB/SPION suspension. Taking together the collected data, the first evidence is that, since the same SPION and surfactant concentration as well as operating conditions were adopted for SPION functionalization, the different behavior of the three systems is ascribable only to the different aggregation properties of the used surfactants.

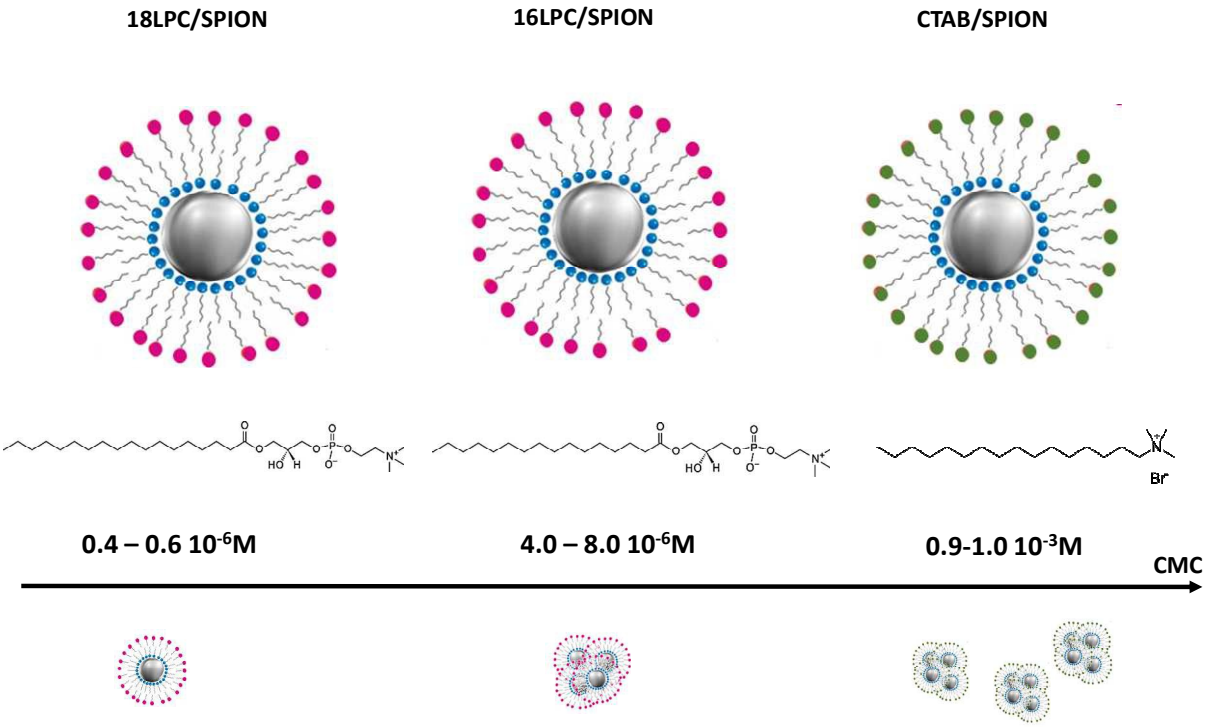

Figure 4: Schematic representation of SPIONs and surfactant structures. The clustering tendency is represented as function of surfactant CMC values.

SPIONs functionalization through hydrophobic interactions is a process strongly associated to the self-aggregation properties of the used surfactant. Indeed, for micellar aggregates, the aggregation tendency of an amphiphilic molecule can be thermodynamically described in terms of a difference in the standard chemical potentials, between the single surfactant molecules dispersed in the solution and those ones within the aggregate. This difference, accounting for the number of

molecules involved in the process, represents the gain of Gibbs free energy of the aggregate formation and is strictly related to a characteristic concentration, known as Critical Micelle Concentration (CMC).The CMC corresponds to the specific surfactant concentration above which the surfactant self-assembles into micelles, in the approximation of the phase separation model.[44] At high CMC values, the aggregation free energy is small and, thus, the surfactants present a poor tendency to self-aggregate. On the other hand, at low CMC values, the aggregation free energy is large and consequently the aggregate formation is the thermodynamically favorite condition for the surfactant molecules.

18LPC and 16LPC are characterized by a CMC value in the range of $0.4\text{-}0.6\cdot10^{-6}$M and $4.0\text{-}8.0\cdot10^{-6}$ M respectively. The different CMC value indicates that 18LPC molecules are less stable in water solution and thus exhibit a larger tendency to self-assemble with respect to 16LPC. This different behavior is, of course, related to the longer hydrophobic tail of 18LPC, since both 18LPC and 16LPC share the same polar head. CTAB is characterized by a CMC value in the range of $0.9\text{-}1.0\cdot10^{-3}$ M, significantly higher than both 18LPC and 16LPC. CTAB CMC is connected with cationic polar head of the surfactant inducing micelle formation only at relatively high surfactant concentration. Thus, the three surfactants used to prepare functionalized SPIONs are characterized by increasing CMC values, and thus decreasing aggregation tendency, in the following order 18LPC<16LPC<CTAB. On these grounds, the description of the aggregation process considered for the surfactant solutions can be adopted for the SPION surface functionalization. Similarly, a coating free energy can be introduced as the difference in terms of chemical potentials between the surfactant molecules in the SPION coating layer and the surfactant molecules dispersed in solution. A small value of this difference reflects a less efficient SPION surface coverage by the surfactant molecules. Thus, the different aggregation behavior is related to the surfactant efficiency in coating the SPIONs and stabilizing them as single functionalized SPIONs or clusters. As a result, while 18LPC/SPIONs are stable in aqueous media as single functionalized nanoparticles, 16LPC/SPIONs and CTAB/SPIONs are characterized by an increasing amount of clusters. This reflects the increasing inefficiency of the surfactant molecules in coating the hydrophobic SPIONs since the surfactant aggregation tendency is lower.

4. Conclusions

SPIONs functionalization through hydrophobic interaction represents an efficient approach to obtain stable SPION aqueous suspensions. Furthermore, it offers the possibility to be easily extended to different kind of amphiphilic molecules, for functionalized SPIONs application in multimodal imaging as well as drug delivery. In this context, the use of zwitterionic surfactants has

emerged as a promising alternative to modified-PEG molecules already approved by FDA. Here we have reported a physico-chemical characterization of three differently surfactant-functionalized SPIONs, underlining the influence of surfactant aggregation properties on the SPION clustering. We have used two zwitterionic phosphocholines and a cationic surfactant in order to explore both the effect of different hydrophilic and hydrophobic molecular regions. In particular, the relation between the surfactant structure, which does determine its CMC value, and the formation of clusters upon the functionalization of the SPIONs was investigated. We have found that the surfactant with the lowest CMC, 18LPC, resulted to be the most efficient in coating the SPIONs leading to a monodispersed aqueous suspension. On the other hand, increasing the surfactant CMC by adopting 16LPC or CTAB, an increasing SPION clustering was observed.

According to the growing interest in surfactant-functionalized SPIONs, the present work furnishes fundamental information about the supramolecular organization of these biomedical nanoparticles, useful to rationally design and optimize SPION preparation.

Acknowledgements

We thank MIUR (PRIN 2010-BJ23MN_007) for financial support and ISIS at the STFC Rutherford Appleton Laboratory for providing the beam time.

Graphical Abstract

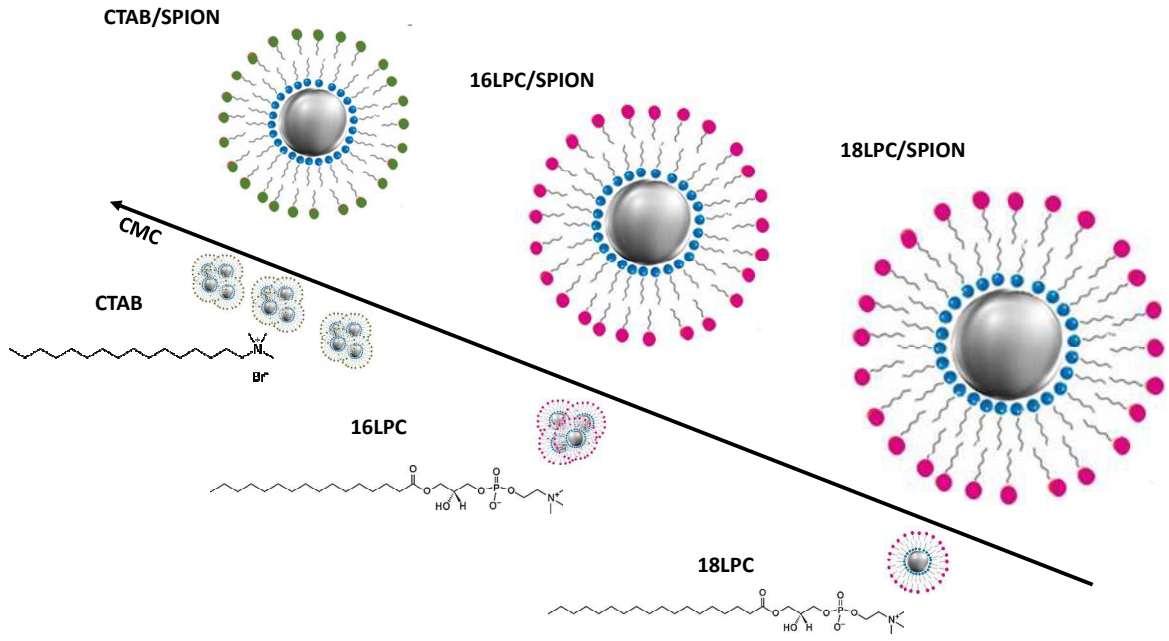

References

1. H. Arami, A. Khandhar, D. Liggitt and K. M. Krishnan, *Chemical Society reviews*, 2015, 44, 8576-8607.
2. E. K. Lim, T. Kim, S. Paik, S. Haam, Y. M. Huh and K. Lee, *Chemical reviews*, 2015, 115, 327-394.
3. N. Lee, D. Yoo, D. Ling, M. H. Cho, T. Hyeon and J. Cheon, *Chemical reviews*, 2015, 115, 10637-10689.
4. H. Wang, X. Zhao, W. Meng, P. Wang, F. Wu, Z. Tang, X. Han and J. P. Giesy, *Analytical chemistry*, 2015, 87, 7667-7675.
5. A. Campanella, Z. Di, A. Luchini, L. Paduano, A. Klapper, M. Herlitschke, O. Petracic, M. S. Appavou, P. Muller-Buschbaum, H. Frielinghaus and D. Richter, *Polymer*, 2015, 60, 176-185.
6. L. Wu, B. Shen and S. Sun, *Nanoscale*, 2015, 7, 16165-16169.
7. D. Wang, C. Deraedt, J. Ruiz and D. Astruc, *Accounts Chem Res*, 2015, 48, 1871-1880.
8. D. Ramimoghadam, S. Bagheri and S. B. Abd Hamid, *Colloids and surfaces. B, Biointerfaces*, 2015, 133, 388-411.
9. F. Y. Dai, M. H. Du, Y. G. Liu, G. Y. Liu, Q. J. Liu and X. Zhang, *J Mater Chem B*, 2014, 2, 2240-2247.
10. M. Vaccaro, G. Mangiapia, L. Paduano, E. Gianolio, A. Accardo, D. Tesauro and G. Morel, *Chemphyschem*, 2007, 8, 2526-2538.
11. Y. Tang, C. Zhang, J. Wang, X. Lin, L. Zhang, Y. Yang, Y. Wang, Z. Zhang, J. W. Bulte and G. Y. Yang, *Advanced functional materials*, 2015, 25, 1024-1034.
12. L. Zhang, W. F. Dong and H. B. Sun, *Nanoscale*, 2013, 5, 7664-7684.
13. C. S. Chiang, Y. H. Tseng, B. J. Liao and S. Y. Chen, *Advanced healthcare materials*, 2015, 4, 1066-1075.
14. C. Niu, Z. Wang, G. Lu, T. M. Krupka, Y. Sun, Y. You, W. Song, H. Ran, P. Li and Y. Zheng, *Biomaterials*, 2013, 34, 2307-2317.
15. G. S. Demirer, A. C. Okur and S. Kizilel, *J Mater Chem B*, 2015, 3, 7831-7849.
16. W. Wei, W. Zhaohui, Y. Taekyung, J. Changzhong and K. Woo-Sik, *Science and Technology of Advanced Materials*, 2015, 16, 023501.
17. S. H. Sun, H. Zeng, D. B. Robinson, S. Raoux, P. M. Rice, S. X. Wang and G. X. Li, *Journal of the American Chemical Society*, 2004, 126, 273-279.
18. H. Groult, J. Ruiz-Cabello, A. V. Lechuga-Vieco, J. Mateo, M. Benito, I. Bilbao, M. P. Martínez-Alcázar, J. A. Lopez, J. Vázquez and F. F. Herranz, *Chemistry – A European Journal*, 2014, 20, 16662-16671.
19. Z. W. Wei Wu, Taekyung Yu, Changzhong Jiang and Woo-Sik Kim, *Chemical Engineering Journal*, 2016, 285, 497.
20. T. Hyeon, S. S. Lee, J. Park, Y. Chung and H. Bin Na, *Journal of the American Chemical Society*, 2001, 123, 12798-12801.
21. A. Luchini, G. Vitiello, F. Rossi, O. Ruiz De Ballesteros, A. Radulescu, G. D'Errico, D. Montesarchio, C. de Julian Fernandez and L. Paduano, *Physical chemistry chemical physics : PCCP*, 2015, 17, 6087-6097.
22. E. Maltas and M. Ozmen, *Materials science & engineering. C, Materials for biological applications*, 2015, 54, 43-49.
23. B. Liu and J. Liu, *Nanoscale*, 2015, 7, 13831-13835.
24. V. Pourcelle, S. Laurent, A. Welle, N. Vriamont, D. Stanicki, L. Vander Elst, R. N. Muller and J. Marchand-Brynaert, *Bioconjugate chemistry*, 2015, 26, 822-829.
25. M. Rahman, Y. Nahar, W. Ullah, A. Elaissari and H. Ahmad, *J Polym Res*, 2015, 22.
26. H. Li, L. Qin, Y. Feng, L. Hu and C. Zhou, *Journal of Magnetism and Magnetic Materials*, 2015, 384, 213-218.

27. S. L. Jeon, M. K. Chae, E. J. Jang and C. Lee, *Chem-Eur J*, 2013, 19, 4217-4222.
28. D. Ling, N. Lee and T. Hyeon, *Accounts Chem Res*, 2015, 48, 1276-1285.
29. S. Mondini, M. Leonzino, C. Drago, A. M. Ferretti, S. Usseglio, D. Maggioni, P. Tornese, B. Chini and A. Ponti, *Langmuir*, 2015, 31, 7381-7390.
30. E. Muro, T. Pons, N. Lequeux, A. Fragola, N. Sanson, Z. Lenkei and B. Dubertret, *Journal of the American Chemical Society*, 2010, 132, 4556-+.
31. D. Kim, M. K. Chae, H. J. Joo, I. H. Jeong, J. H. Cho and C. Lee, *Langmuir*, 2012, 28, 9634-9639.
32. Z. G. Estephan, J. A. Jaber and J. B. Schlenoff, *Langmuir*, 2010, 26, 16884-16889.
33. G. Vitiello, D. Ciccarelli, O. Ortona and G. D'Errico, *Journal of colloid and interface science*, 2009, 336, 827-833.
34. A. Luchini, C. Irace, R. Santamaria, D. Montesarchio, R. K. Heenan, N. Szekely, A. Flori, L. Menichetti and L. Paduano, *Nanoscale*, 2016, DOI: 10.1039/c5nr08486e.
35. B. J. P. Berne, R., *Dynamic Light Scattering: With Applications to Chemistry, Biology, and Physics*, Couvire Dover Publications, 2000.
36. A. Lomakin, D. Teplow and G. Benedek, in *Amyloid Proteins*, ed. E. Sigurdsson, Humana Press, 2005, vol. 299, ch. 10, pp. 153-174.
37. B. J. B. a. R. Pecora, *Dynamic Light Scattering: With Applications to Chemistry, Biology, and Physics* Couvire Dover Publications, 2003.
38. J. S. H. a. H. C. Benoit, *Polymers and Neutron Scattering*, Clarendon Press, 1997.
39. P. Roscigno, L. Paduano, G. D'Errico and V. Vitagliano, *Langmuir*, 2001, 17, 4510-4518.
40. M. Kotlarchyk and S. H. Chen, *The Journal of Chemical Physics*, 1983, 79, 2461-2469.
41. D. G. Leaist, *J Colloid Interf Sci*, 1986, 111, 230-239.
42. O. Annunziata, L. Costantino, G. D'Errico, L. Paduano and V. Vitagliano, *J Colloid Interf Sci*, 1999, 216, 16-24.
43. O. Annunziata, L. Costantino, G. D'Errico, L. Paduano and V. Vitagliano, *J Colloid Interf Sci*, 1999, 216, 8-15.
44. H. Wennerström, J. Morris and U. Olsson, *Langmuir*, 1997, 13, 6972-6979.